Electronic supplementary material - ESI

Sensitization of lanthanide complexes through direct spin-forbidden singlet→triplet excitation

Airton G. Bispo-Jr,[a] Italo O. Mazali,[a] and Fernando A. Sigoli*[a]

[a.] *Department of inorganic chemistry, Institute of Chemistry, University of Campinas, Unicamp, Josué de Castro street, Cidade Universitária, Campinas, 13083-970*

Table of Contents

Supplementary note S1. Spin-orbital coupling parameter

Table S1. Spin-orbital coupling parameter (ζ).

Element	ζ / cm^{-1}	[reference]
C	58	[1]
Cl	564	[1]
Br	2,420	[1]
Eu	1,326	[2]
Tb	1,709	[2]
Er	2,241	[3]
Yb	2,884	[4]

Supplementary note S2 - Experimental Procedures

Terbium oxide (Tb_4O_7, Aldrich, 99.9%), europium oxide (Eu_2O_3, Aldrich, 99.9%), gadolinium oxide (Gd_2O_3, Aldrich, 99.9%), ytterbium oxide (YbO_3, Aldrich, 99.9%), erbium oxide (Er_2O_3, Aldrich, 99.9%), hydrogen peroxide (H_2O_2, Synth, 34-46%), hydrochloric acid (HCl, Synth, 36%), sodium hydroxide (NaOH, Synth, 98%), benzoic acid (Aldrich, 99.5%), 4-clorobenzoic acid ($ClC_6H_4CO_2H$, Aldrich, 99%), 4-bromobenzoic acid ($BrC_6H_4CO_2H$, Aldrich, 98%), 3,5-diclorobenzoic acid ($Cl_2C_6H_3CO_2H$, Aldrich, 97%), and 3,5-dibromobenzoic acid ($Br_2C_6H_3CO_2H$, Aldrich, 95%) were used as starting reactants without any further purification.

First, aqueous lanthanide chloride solutions (*pH* = 5) were prepared by dissolving the Ln_2O_3 (or Tb_4O_7) in a stoichiometric amount of hot (80 °C) hydrochloric acid solution (1 mol L^{-1}) according to Equation S1. For the complete dissolution of Tb_4O_7, some drops of H_2O_2 were added to the reaction. The $LnCl_3$ solution was titrated by the EDTA method using solid ortho-xylenol orange (3wt.% in KBr) as an indicator.

$$Ln_2O_{3(s)} + 6HCl_{(aq)} \rightarrow 2LnCl_{3(aq)} + 3H_2O_{(l)} \quad (S1)$$

For complex syntheses, 1.5 mmol of ligand was added in 15 mL of water, and the suspension was heated at 80 °C. After that, a stoichiometric amount of NaOH (1.5 mmol, 1 mol L^{-1}) was added to deprotonate the carboxylate group, keeping heating up to the total dissolution. The *pH* was then corrected to 6 with HCl (0.1 mol L^{-1}). In the sequence, this solution was added in 0.5 mmol of $LnCl_3$ aqueous solution (ligand:Ln^{III} mol proportion of 3:1), which was kept upon magnetic stirring for 30 min at 80 °C. The complex was obtained as a white powder that was filtered, washed with cold water, and dried in a desiccator at 25 °C. The synthesis yield was close to 80% for all complexes. A general scheme for complex syntheses and pictures of representative Eu^{III} or Tb^{III} complexes upon UV radiation exposition are shown in Figure S1. Er^{III} and Yb^{III} complexes with bza^-, $4\text{-}cbza^-$, and $4\text{-}bbza^-$ ligands were not prepared because these ligands do not enable a direct triplet state population. Eu^{III}, Tb^{III}, and Gd^{III} complexes with bbza, 4-cbza, 4-bbza, and 3,5-bbza ligands have already been reported by Monteiro and co-workers[5] while Yb^{III} and Er^{III} complexes as well as all with 3,5-bbza ligands have not been reported yet.

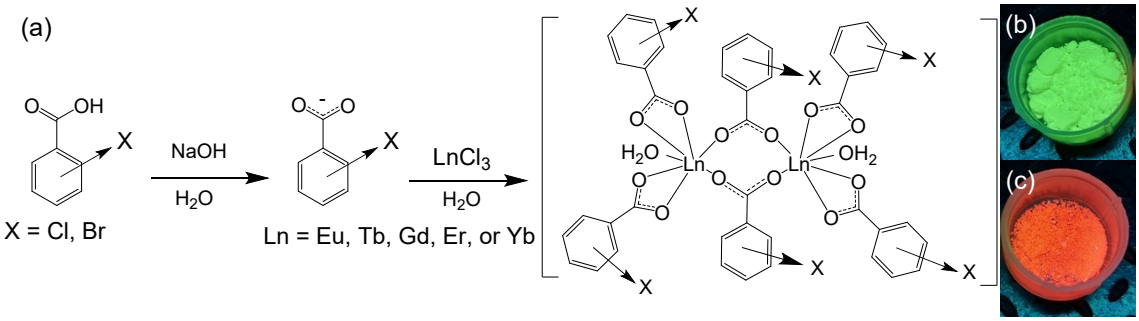

Figure S1. (a) Reaction steps for the syntheses of $[Ln(X\text{-}bza)_3(H_2O)_2]_2$ complexes. Pictures of (b) $[Tb_2(3,5\text{-}cbza)_6(H_2O)_2]$ and (c) $[Eu_2(3,5\text{-}cbza)_6(H_2O)_2]$ upon UV (365 nm) radiation exposition.

Characterization

FTIR. FTIR measurements of powder complexes were carried out in a FTIR Agilent Cary 630 spectrophotometer in the ATR (attenuated total reflectance) mode with an increment of 2 cm^{-1}.

Diffuse reflectance spectroscopy. Diffuse reflectance spectra (DRS) in the absorbance mode were obtained for powder complexes using a SHIMADZU UV-2450 equipment with integrating sphere, increment of 1 nm, and $BaSO_4$ as reflectance standard (see reflectance spectrum in Figure S2).

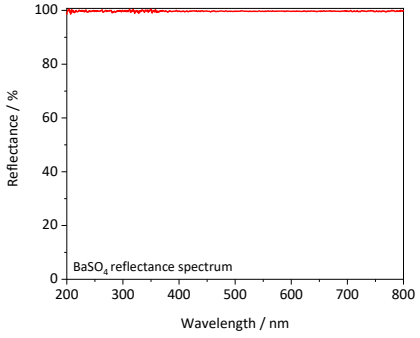

Figure S2. Reflectance spectrum of $BaSO_4$ pattern ensuring that no scattering bands take place during the DRS measurement.

Steady-state photoluminescence. The photoluminescence data were obtained in a Fluorolog-3 spectrofluorometer (Horiba FL3-22-iHR320), with double-gratings (1200 g/mm, 330 nm blaze) in the excitation monochromator and double-gratings (1200 g/mm, 500 nm blaze) in the emission monochromator. An ozone-free Xenon lamp of 450 W (Ushio) was used as a radiation source. The excitation spectra were corrected in real time according to the lamp intensity and the optical system of the excitation monochromator using a silicon diode as a reference. The emission spectra were carried using the front face mode at 22.51°. All of them were corrected according to the optical system of the emission monochromator and the photomultiplier response (Hamamatsu R928P). Excitation and emission slits were kept close to 0.5 mm for all spectra and increments of 0.5 nm. For Yb^{III} samples, emission spectra were carried out using an emission iHR320 monochromator (1200 g/mm, 330 nm blaze) and a CCD Sdrive-500 Horiba camera, while excitation spectra were measured using a Hamamatsu H10330-75 detector (same of Er^{III} complexes).

Time-resolved luminescent spectroscopy. Time-resolved spectroscopy was obtained by using a 150 W xenon lamp and a Time-Correlated Single Photon Count (TCSPC) system equipped in the Horiba FL3-22-iHR320 spectrofluorometer at 298 K. All emission decay curves were measured in triplicate and adjusted by a monoexponential decay function, whereas the emitting state lifetimes were determined as an average of measurements.

Emission spectroscopy of Gd^{III} complexes at 77 K. Excitation and emission spectra at were measured using the Fluorolog 3 equipment. A THMS600 Linkam system (0.01 °C accuracy) with liquid N_2 was used to control the temperature, and optic fibers conducted the excitation and emission signals (the thermal dependence of luminescence of $[Yb_2(3,5\text{-bbza})_6(H_2O)_2]$ complex was measured by using the same experimental set up).

Complexometric titration of complexes. Specific amounts (Table S2) of complexes were dissolved in hot (80 °C) HCl (1 mol L^{-1}) to break the Ln^{III} – ligand bond. After that, 10 mL of Hac/ac^- (ac^- = acetate) buffer (*pH* = 5) was added followed by the indicator ortho-xylenol orange (3wt.% in KBr). The solution was then titrated with 0.01 mol L^{-1} EDTA by using an electronic burette with 0.01 mL accuracy. The titration was performed in triplicate.

Table S2. Complexometric titration of $[Ln_2(X\text{-cbza})_6(H_2O)_2]$ complexes representing the theoretical molecular weight (MW), weight of complex, and theoretical and experimental EDTA volume consumed during the process. [EDTA] = 0.01 mol L^{-1}.

Complex	MW / g mol^{-1}	Weight / mg	V_{EDTA} theoretical / mL	V_{EDTA} experimental / ± 0.02 mL
$[Gd_2(bza)_6(H_2O)_2]$	1077.22	11.5	2.12	2.04
$[Eu_2(bza)_6(H_2O)_2]$	1066.64	25.0	4.69	4.58
$[Tb_2(bza)_6(H_2O)_2]$	1080.28	13.0	2.41	2.37
$[Gd_2(4\text{-cbza})_6(H_2O)_2]$	1283.92	23.0	3.58	3.43
$[Eu_2(4\text{-cbza})_6(H_2O)_2]$	1273.34	23.0	3.60	3.48
$[Tb_2(4\text{-cbza})_6(H_2O)_2]$	1287.26	23.1	3.58	3.53
$[Gd_2(4\text{-bbza})_6(H_2O)_2]$	1550.62	24.8	3.21	3.16
$[Eu_2(4\text{-bbza})_6(H_2O)_2]$	1540.94	19.1	2.47	2.45
$[Tb_2(4\text{-bbza})_6(H_2O)_2]$	1553.96	28.0	3.58	3.48
$[Gd_2(3,5\text{-cbza})_6(H_2O)_2]$	1496.62	29.6	3.95	3.83
$[Eu_2(3,5\text{-cbza})_6(H_2O)_2]$	1486.06	32.4	4.36	4.30
$[Tb_2(3,5\text{-cbza})_6(H_2O)_2]$	1536.06	28.5	3.71	3.70
$[Yb_2(3,5\text{-cbza})_6(H_2O)_2]$	1500.14	22.3	2.97	2.90
$[Er_2(3,5\text{-cbza})_6(H_2O)_2]$	1510.58	24.7	3.26	3.16
$[Gd_2(3,5\text{-bbza})_6(H_2O)_2]$	2030.00	22.5	2.21	2.15
$[Eu_2(3,5\text{-bbza})_6(H_2O)_2]$	2033.20	21.6	2.12	2.02
$[Tb_2(3,5\text{-bbza})_6(H_2O)_2]$	2019.40	19.1	1.89	1.80
$[Yb_2(3,5\text{-bbza})_6(H_2O)_2]$	2055.60	25.4	2.47	2.46
$[Er_2(3,5\text{-bbza})_6(H_2O)_2]$	2044.00	20.2	1.97	1.90

Elemental analysis. C, H, N elemental analysis of complexes were measured in triplicate in a PerkinElmer® 2400 Series II CHNS/O Elemental Analyzer (2400 Series II), Results for all complexes are displayed in Table S3.

Table S3. Elemental analysis (C, H) of complexes.

Complex	C_{theo} / %	C_{exp} / %	H_{theo} / %	H_{exp} / %
$[Gd_2(bza)_6(H_2O)_2]$	46.83	48.52	3.18	3.08
$[Eu_2(bza)_6(H_2O)_2]$	47.29	48.25	3.21	2.98
$[Tb_2(bza)_6(H_2O)_2]$	46.68	48.18	3.17	2.99
$[Gd_2(4\text{-}cbza)_6(H_2O)_2]$	39.29	40.18	2.20	2.06
$[Eu_2(4\text{-}cbza)_6(H_2O)_2]$	39.62	40.10	2.22	2.14
$[Tb_2(4\text{-}cbza)_6(H_2O)_2]$	39.19	39.74	2.19	2.10
$[Gd_2(4\text{-}bbza)_6(H_2O)_2]$	32.53	32.78	1.82	1.77
$[Eu_2(4\text{-}bbza)_6(H_2O)_2]$	32.76	32.01	1.83	2.09
$[Tb_2(4\text{-}bbza)_6(H_2O)_2]$	32.62	33.05	1.82	1.70
$[Gd_2(3,5\text{-}cbza)_6(H_2O)_2]$	33.84	34.41	1.48	1.37
$[Eu_2(3,5\text{-}cbza)_6(H_2O)_2]$	34.09	34.64	1.50	1.37
$[Tb_2(3,5\text{-}cbza)_6(H_2O)_2]$	33.77	34.20	1.48	1.38
$[Yb_2(3,5\text{-}cbza)_6(H_2O)_2]$	33.14	32.76	1.46	1.32
$[Er_2(3,5\text{-}cbza)_6(H_2O)_2]$	33.4	33.23	1.47	1.50
$[Gd_2(3,5\text{-}bbza)_6(H_2O)_2]$	24.92	24.50	1.10	1.28
$[Eu_2(3,5\text{-}bbza)_6(H_2O)_2]$	25.06	24.80	1.10	1.16
$[Tb_2(3,5\text{-}bbza)_6(H_2O)_2]$	24.88	25.37	1.09	1.08
$[Yb_2(3,5\text{-}bbza)_6(H_2O)_2]$	24.54	24.71	1.08	1.04
$[Er_2(3,5\text{-}bbza)_6(H_2O)_2]$	24.68	24.61	1.08	1.21

Absolute emission quantum yield. Emission quantum yield (Φ_L^{Ln}) upon 360 nm excitation (singlet → triplet band) was measured in a Quanta -ϕ F-3029 integrating sphere coupled by optic fibers to the previously mentioned fluorimeter. For reference, the empty sphere coated with Spectralon® (reflectance > 95%) was used. The emission quantum yield is given by Equation S2, where N_{Em} and N_{Abs} are the number of photons emitted and absorbed by the sample, respectively, I_{em} is the emission spectrum of the sample, and I_{ex} and I_{ex}^{st} stand for the excitation spectra of the light used to excite the sample and the integrating sphere empty, respectively.

$$\Phi_L^{Ln} = \frac{N_{Emi}}{N_{Abs}} = \frac{\int_{\lambda_1}^{\lambda_2} I_{em}(\lambda)d\lambda}{\int_{\lambda_3}^{\lambda_4} I_{ex}^{st}(\lambda)d\lambda - \int_{\lambda_3}^{\lambda_4} I_{ex}(\lambda)d\lambda} \quad (S2)$$

Relative emission quantum yield. The relative emission quantum yield upon 300 nm excitation (singlet → singlet band) was measured by using quinine sulfate dihydrate (Sigma-Aldrich, meets USP testing specifications) in 0.1 M $HClO_4$ (quantum yield of 59%) as a reference following a standard protocol.[6] For that, emission spectra of reference (*ref.*) and samples (*x*, dissolved in high-purity anhydrous DMF from Sigma-Aldrich) were measured upon the same condition (excitation and emission slits of 0.71 mm, integration time of 0.1 s, and increment of 1 nm) while absorbance (*A*) of all samples was kept below 0.1 to guarantee that samples follow the Lambert-Beer law. All emission spectra were corrected by subtracting the emission spectrum of the pure solvent upon the same excitation conditions. The emission quantum yield was measured in triplicate using Equation S3, where *F* is the integrated emission intensity, *f* is the absorption factor ($f = 1\text{-}10^{-A}$), *n* is the refractive index of the solvent, and *Φ* is the emission quantum yield.

$$\Phi_x = \Phi_{ref.} \frac{F_x \; f_{ref} \; n_x^2}{F_{ref.} \; f_x \; n_{ref}^2} \quad (S3)$$

Singlet and triplet theoretical energy calculations. This calculation was carried out in the LUMPAC software[7] by implementing the MOPAC program.[8] For that, the Sparkle/RM1[9] semi-empirical model was used to determine the ground-state geometries of all ligands by considering the following keywords: SPARKLE PRECISE GEO-OK XYZ T=10D ALLVEC BFGS GNORM=0.25. Excited-state energies from these structures were then calculated in the LUMPAC program using the ORCA software.[10]

Supplementary note S3. FTIR Analyses

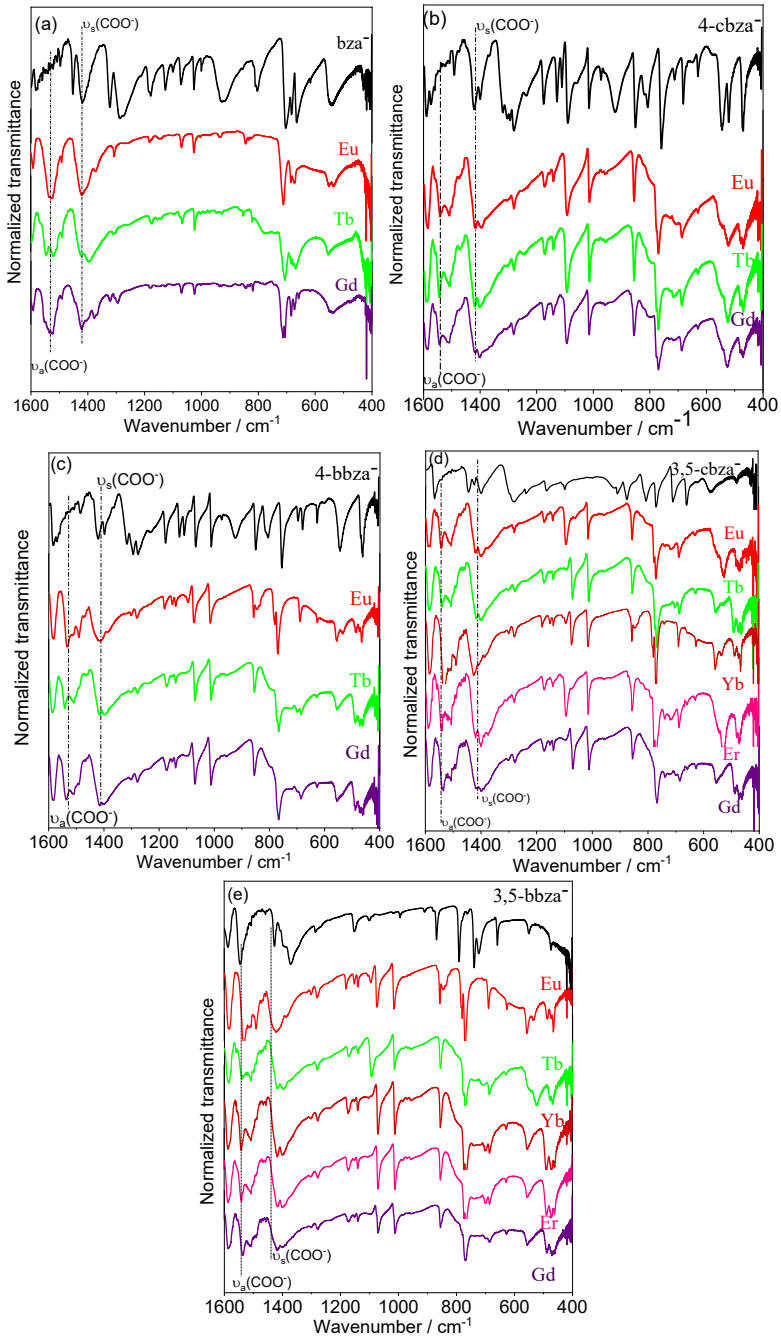

Figure S3. FTIR spectra of (a) $[Ln_2(bza)_6(H_2O)_2]$, (b) $[Ln_2(4\text{-cbza})_6(H_2O)_2]$, (c) $[Ln_2(4\text{-bbza})_6(H_2O)_2]$, (d) $[Ln_2(3,5\text{-cbza})_6(H_2O)_2]$, and (e) $[Ln_2(3,5\text{-bbza})_6(H_2O)_2]$ (Ln = Gd, Eu, Tb, Er, or Yb) compared with the equivalent ligand salt.

In the FTIR spectra represented in Figure S3, the most important vibrational modes noticed are the ν(C=C) stretching at about 1600 cm^{-1}, the δ(C-H) angular deformation peaking at 714 and 683 cm^{-1}, and the asymmetric $\nu_a(COO^-)$ and symmetric $\nu_s(COO^-)$ stretching of carboxylate group at about 1547 and 1417 cm^{-1}, respectively. Notably, the asymmetric $\nu_a(COO^-)$ vibrational mode of ligand salt shifts to shorter energies after coordination, confirming that the COO^- bond distances change, thus, suggesting the complex formation. For all complexes, there is a splitting of the

band attributed to the $\nu_a(COO^-)$ (at about 1,550 cm^{-1}) due to the presence of two different coordination modes, a bridge-like bidentate and chelate mode of coordination, according to Deacon and Phillips,[11] which agrees with the previously determined stoichiometry by complexometric titration and the homobimetallic structures previously reported by J. H. S. K. Monteiro and coworkers.[5]

Supplementary note S4 – Singlet and triplet state energy determination

Table S4. Semi-empirical values of the lowest-energy singlet and triplet levels of ligands were determined via ORCA software. The values are similar for all studied ligands.

S_n	Energy / cm^{-1}	Band position / nm	T_n	Energy / cm^{-1}	Band position / nm
S_1	36,727	272.3	T_1	23,346	428.3
S_2	36,852	271.4	T_2	23,351	428.2
S_3	36,874	271.2	T_3	23,355	428.2
S_4	36,878	271.2	T_4	28,986	345.0
S_5	36,879	271.2	T_5	28,991	344.9
S_6	36,887	271.1	T_6	28,999	344.8
S_7	41,532	240.8	T_7	30,353	329.5

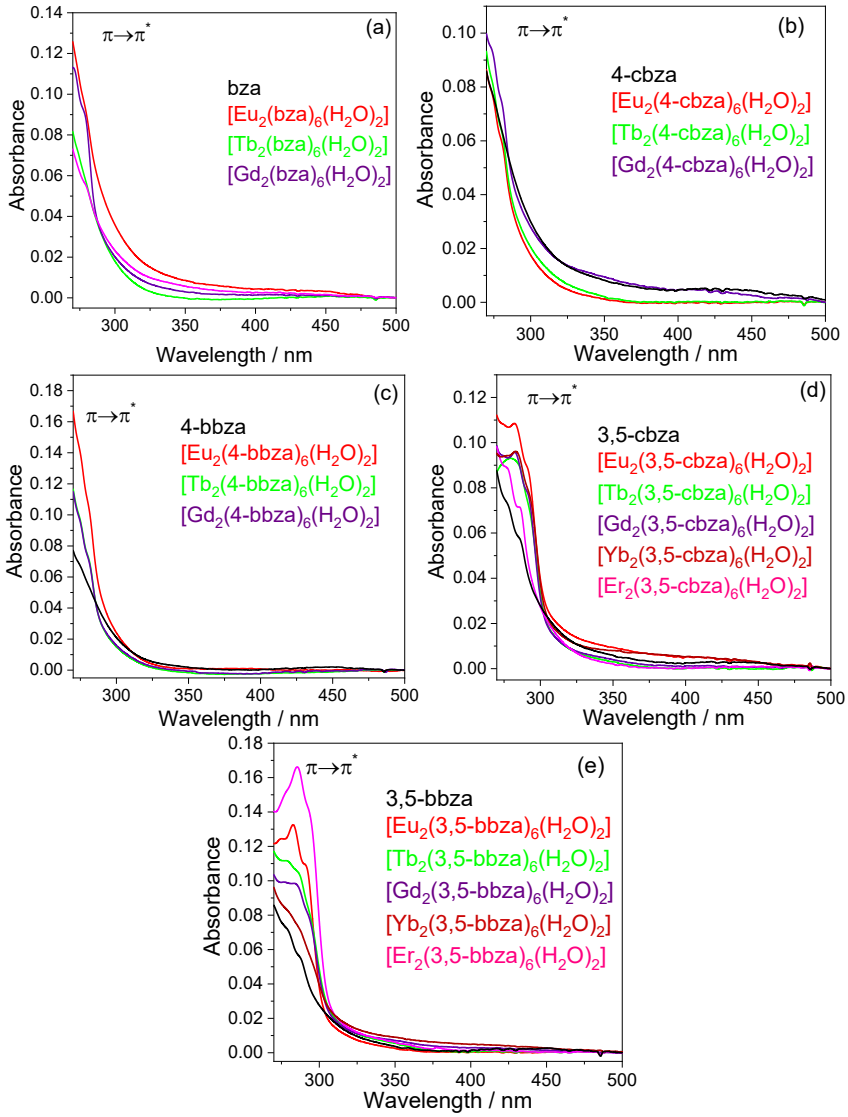

Figure S4. UV-VIS absorption spectra in DMF solutions ($3 \cdot 10^{-5}$ M) of (a) $[Ln_2(bza)_6(H_2O)_2]$, (b) $[Ln_2(4\text{-cbza})_6(H_2O)_2]$, (c) $[Ln_2(4\text{-bbza})_6(H_2O)_2]$, (d) $[Ln_2(3,5\text{-cbza})_6(H_2O)_2]$, and (e) $[Ln_2(3,5\text{-bbza})_6(H_2O)_2]$ (Ln = Gd, Eu, Tb, Er, or Yb) compared with the equivalent ligand salt.

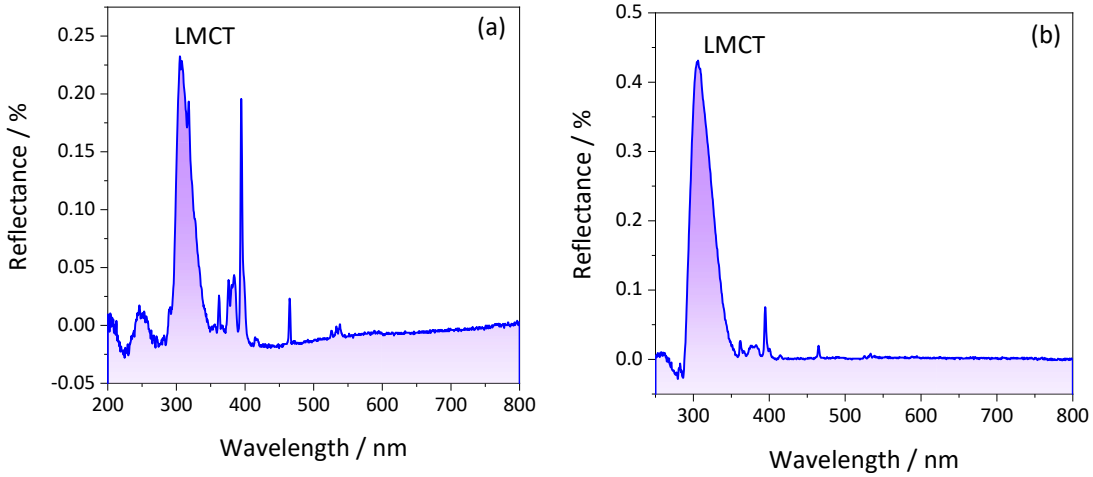

Figure S5. Arithmetic difference between the DRS spectra of (a) $[Eu_2(4\text{-cbza})_6(H_2O)_2]$ and $[Gd_2(4\text{-cbza})_6(H_2O)_2]$ or (b) $[Eu_2(4\text{-bbza})_6(H_2O)_2]$ and $[Gd_2(4\text{-bbza})_6(H_2O)_2]$. Since the DRS spectra of Gd complexes are free of LMCT processes,

they can be used as reference to identify LMCT processes in other Ln complexes by the arithmetic difference between their DRS spectra.

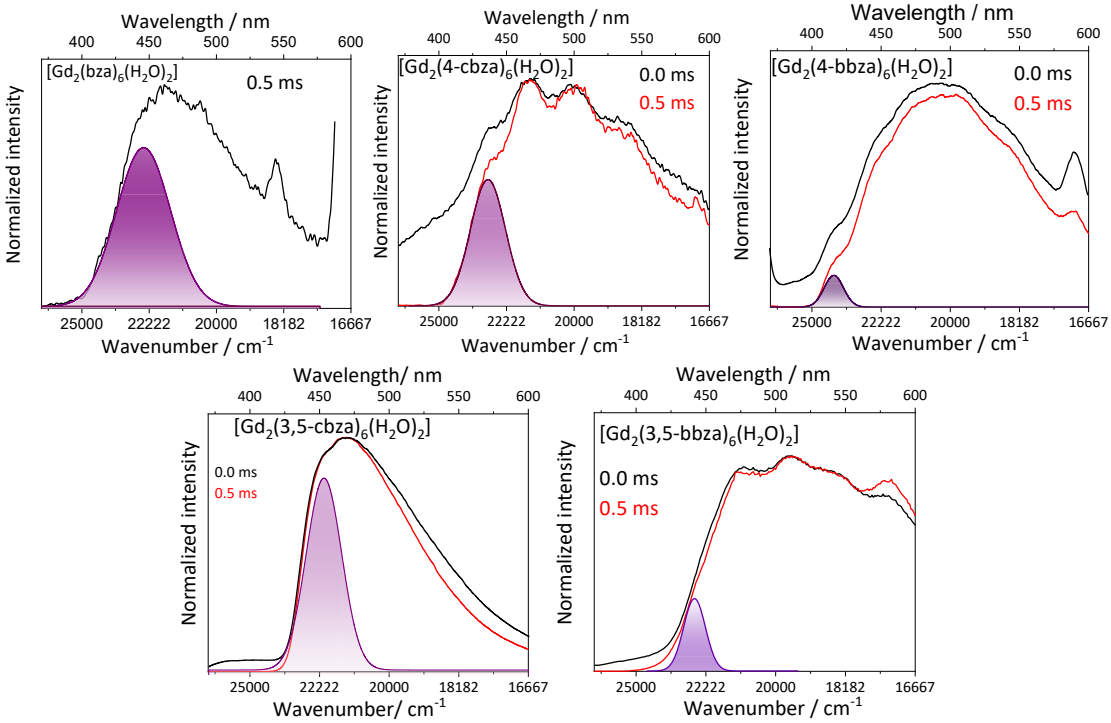

Figure S6. Time-resolved (delay of 0.5 ms) emission spectra (77 K) of Gd^{III} powder complexes compared with the steady-state emission. The deconvolution of each spectrum was carried out by applying a gaussian function. To avoid any emission coming from short-lived singlet excited states or vibronic components, time-resolved emission spectra measured at 77 K were recorded while the zero-phonon transition energy obtained by the band energy maximum was considered for the assignment. The triplet state energy was determined by considering the local maxima of the zero-phonon band. Peaks at 545 and 612 nm are assigned to Tb^{III} or Eu^{III} emissions, respectively, usually found as contaminants in Gd_2O_3 (purity of 99.9%) yet, the band positions of such contaminants do not match the region where emission bands are important for triplet state determination, so, the analyses are not compromised.

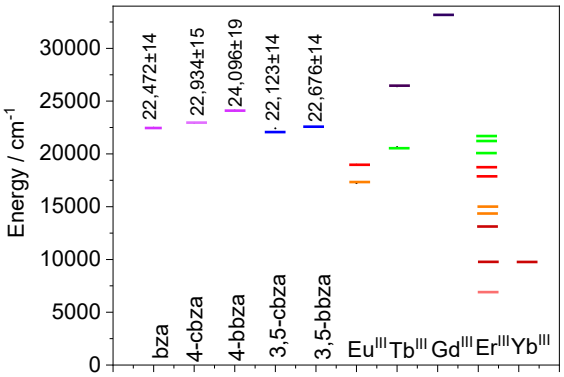

Figure S7. Triplet state energy of ligands compared with the main emitting levels of Tb^{III}, Eu^{III}, Gd^{III}, Er^{III}, and Yb^{III}.

Supplementary note S5 – Emission features of complexes

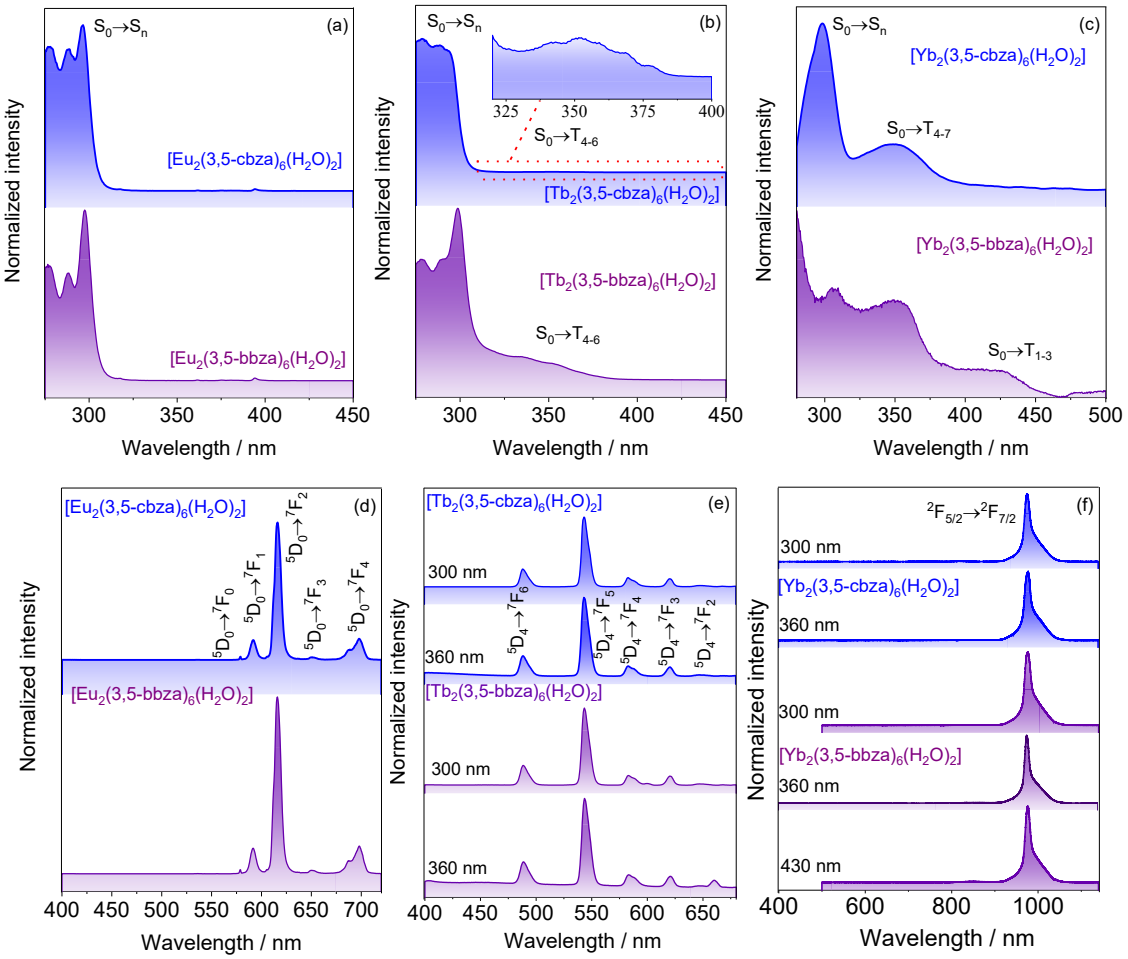

Figure S8. Excitation spectra (298 K) in DMF solution (1 10^{-4} M) of (a) Eu^{III} (λ_{em} = 612 nm), (b) Tb^{III} (λ_{em} = 543 nm), and (c) Yb^{III} (λ_{em} = 980 nm) complexes, and emission spectra in DMF solution (1 10^{-4} M) of (d) Eu^{III} (λ_{exc} = 300 nm), (e) Tb^{III} (λ_{exc} = 300 or 360 nm), and (f) Yb^{III} (λ_{ex} = 300, 360, or 430 nm) complexes with 3,5-cbza or 3,5-bbza ligands.

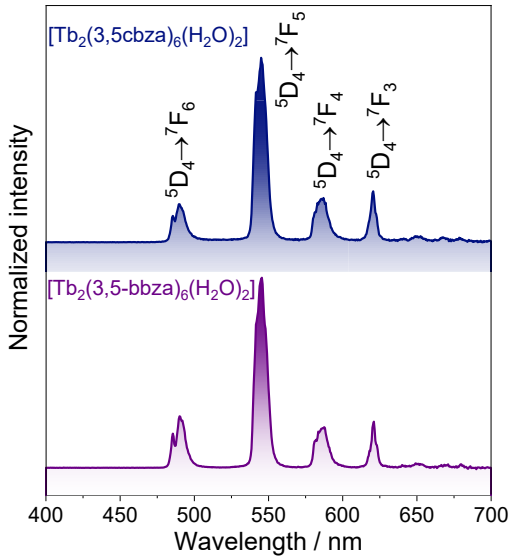

Figure S9. Emission spectra (298 K) of $[Tb_2(3,5\text{-cbza})_6(H_2O)_2]$ and $[Tb_2(3,5\text{-bbza})_6(H_2O)_2]$ powder complexes (λ_{exc} = 360 nm).

Supplementary note S6 – Time-resolved spectroscopy

Table S5. Eu^{III} $^5D_0$ and Tb^{III} $^5D_4$ emitting states lifetimes measured at 298 K for powder complexes or in DMF solution (1 10^{-4} M). The monitored excitation (λ_{exc}) and emission (λ_{em}) wavelengths are also represented. The emitting state lifetime is a kinetic constant that enables a deep analysis of the deactivation process of a state through non-radiative (A_{nrad}) and radiative (A_{rad}) decay probabilities, $\tau = (A_{total})^{-1} = (A_{rad}+A_{nrad})^{-1}$.

Complex	λ_{exc} / nm	λ_{em} / nm	State	τ_{powder} / ms	τ_{DMF} / ms
$[Eu_2(bza)_6(H_2O)_2]$	290	615	$^5D_0$	0.39	0.56
$[Eu_2(4\text{-}cbza)_6(H_2O)_2]$	280	613	$^5D_0$	0.24	0.57
$[Eu_2(4\text{-}bbza)_6(H_2O)_2]$	280	615	$^5D_0$	0.44	0.54
$[Eu_2(3,5\text{-}cbza)_6(H_2O)_2]$	309	615	$^5D_0$	0.44	0.62
$[Eu_2(3,5\text{-}bbza)_6(H_2O)_2]$	300	615	$^5D_0$	0.39	0.62
$[Tb_2(bza)_6(H_2O)_2]$	280	543	$^5D_4$	0.73	1.31
$[Tb_2(4\text{-}cbza)_6(H_2O)_2]$	280	543	$^5D_4$	0.72	0.93
$[Tb_2(4\text{-}bbza)_6(H_2O)_2]$	280	543	$^5D_4$	0.69	1.17
$[Tb_2(3,5\text{-}cbza)_6(H_2O)_2]$	303/360	543	$^5D_4$	1.24/ 1.21	1.11/0.95
$[Tb_2(3,5\text{-}bbza)_6(H_2O)_2]$	303/360	543	$^5D_4$	0.84/ 0.73	1.03/0.94

Table S6. Er^{III} $^4I_{13/2}$ and Yb^{III} $^2F_{5/2}$ emitting state lifetime measured at 298 K for powder complexes. The monitored excitation (λ_{exc}) and emission (λ_{em}) wavelengths are also represented.

Complex	λ_{exc} / nm	λ_{em} / nm	State	τ / µs
$[Yb_2(3,5\text{-}cbza)_6(H_2O)_2]$	300/360	980	$^2F_{5/2}$	68/70
$[Yb_2(3,5\text{-}bbza)_6(H_2O)_2]$	300/360/430	980	$^2F_{5/2}$	25/22/21
$[Er_2(3,5\text{-}cbza)_6(H_2O)_2]$	300	1537	$^4I_{13/2}$	2.63
$[Er_2(3,5\text{-}bbza)_6(H_2O)_2]$	300/360	1537	$^4I_{13/2}$	3.0/3.3

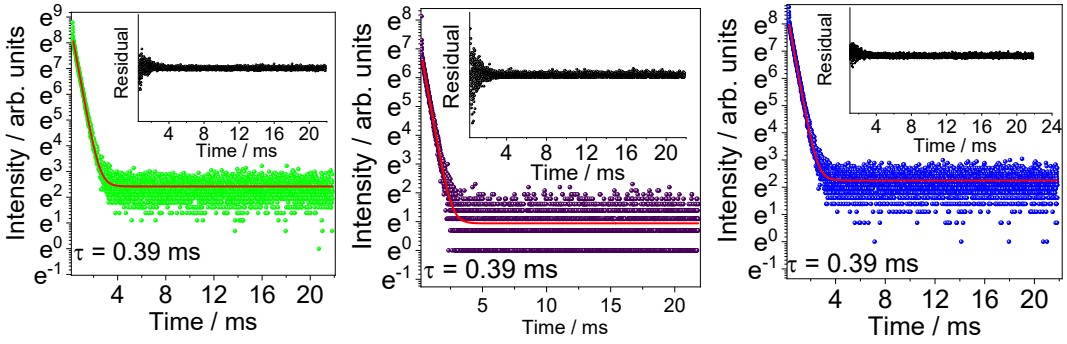

Figure S10. Emission intensity decay curves of $[Eu_2(3,5\text{-}bbza)_6(H_2O)_2]$ powder complex monitored at 293 K. (λ_{exc} = 300 nm, λ_{em} = 612 nm). Curves were fitted through a monoexponential adjustment ($R^2 > 0.95$), and the residual plots are represented as an insert in each image.

Supplementary note S7 – Photophysical parameters

For Eu^{III} complexes, experimental Ω_2 and Ω_4 (Equation S4) Judd-Ofelt intensity parameters, radiative (Equation S5) and non-radiative decay probabilities (A), and intrinsic emission quantum yield (Φ_{Eu}^{Eu}, Equation S6) were obtained from the emission spectrum through the LUMPAC® software. In these equations, ω is the angular frequency of incident radiation, $\chi = n(n+2)^2/9$ is the Lorentz local-field correction, n is the refractive index of the medium (1.500), $\left|\left\langle {}^7F_J \middle\| U^{(\lambda)} \middle\| {}^5D_0 \right\rangle\right|^2$ is 0.0032 or 0.0023 for J = 2 and 4, respectively, $A_{0\lambda}$ is the spontaneous emission probability, $A_{01}=14,6\cdot n^3$, τ is the emitting state lifetime, and S_{0J} is the area under the band assigned to the $^5D_0 \rightarrow {}^7F_J$ transition. In this approach, the Ω_6 parameter is not calculated because the $^5D_0 \rightarrow {}^7F_6$ transition is not observed in the monitored emission range.

$$\Omega_\lambda = \frac{3hc^3 A_{0\lambda}}{8\pi e^2 \omega^3 \chi \left|\left\langle {}^7F_J \middle\| U^{(\lambda)} \middle\| {}^5D_0 \right\rangle\right|^2} (S4)$$

$$A_{0J} = A_{01}\left(\frac{v_{01}}{v_{0J}}\right)\left(\frac{S_{0J}}{S_{01}}\right) (S5)$$

$$\Phi_{Eu}^{Eu} = \frac{A_{rad}}{A_{Total}} = \frac{\tau_{total}}{\tau_{rad}} (S6)$$

Regarding Ω_2 parameter, the value changes for all complexes due to modifications of Eu^{III} local microssymetry since it is more influenced by variations of Eu^{III} – ligand (L) bond angles, Table S7.[12] On the other hand, the Ω_4 parameter, which is related to the polarizability of ligand species and may be correlated with variations in the Eu^{III} – L bond distance, also differs for each complex, ensuring modifications of Eu^{III} – L bond distance and polarizability of ligands.[12]

Table S7. Judd-Ofelt Ω_2 and Ω_4 intensity parameters, radiative (A_{rad}) and non-radiative (A_{nrad}) decay probabilities, and intrinsic emission quantum yield (Φ_{Eu}^{Eu}) of Eu^{III} powder complexes.

Complex	Ω_2 / 10^{-20} cm^2	Ω_4 / 10^{-20} cm^2	A_{rad} / s^{-1}	A_{nrad} / s^{-1}	Φ_{Eu}^{Eu} / %
$[Eu_2(bza)_6(H_2O)_2]$	8.2	5.8	382	2189	15
$[Eu_2(4\text{-}cbza)_6(H_2O)_2]$	7.0	5.2	345	3749	8.4
$[Eu_2(4\text{-}bbza)_6(H_2O)_2]$	5.0	1.6	234	2018	10
$[Eu_2(3,5\text{-}cbza)_6(H_2O)_2]$	6.2	6.4	331	1925	15
$[Eu_2(3,5\text{-}bbza)_6(H_2O)_2]$	7.1	6.4	355	2171	14

The intrinsic emission quantum yield of samples (Φ_{Eu}^{Eu}) barely changes for all complexes except for $[Eu_2(4\text{-}cbza)_6(H_2O)_2]$. The value is relatively low due to the high contribution of non-radiative processes, as represented by A_{nrad} in Table S7. This substantial contribution of non-radiative pathways comes from the two coordinated water molecules bonded to each metallic center, as previously determined by complexometric titration. Water molecules lead to non-radiative deactivation of the $^5D_0$ state due to multiphonon interactions caused by O-H oscillators.[13]

Table S8. Overall emission quantum yield (Φ_L^{Ln}) of Eu^{III} and Tb^{III} complexes.

Complex	Φ_L^{Ln} / %[a]	Φ_L^{Ln} / %[b]	Complex	Φ_L^{Ln} / %[a]	Φ_L^{Ln} / %[b]
$[Eu_2(bza)_6(H_2O)_2]$	< 1	< 1	**$[Tb_2(bza)_3(H_2O)_2]$**	13	< 1
$[Eu_2(4\text{-}cbza)_6(H_2O)_2]$	2	< 1	**$[Tb_2(4\text{-}cbza)_6(H_2O)_2]$**	< 1	3.7±0.4
$[Eu_2(4\text{-}bbza)_6(H_2O)_2]$	< 1	< 1	**$[Tb_2(4\text{-}bbza)_6(H_2O)_2]$**	< 1	<1
$[Eu_2(3,5\text{-}cbza)_6(H_2O)_2]$	10	< 1	**$[Tb_2(3,5\text{-}cbza)_6(H_2O)_2]$**	**2**	**18±2**
$[Eu_2(3,5\text{-}bbza)_6(H_2O)_2]$	< 1	<1	**$[Tb_2(3,5\text{-}bbza)_6(H_2O)_2]$**	**8**	**12±1**

[a] Relative emission quantum yield measured upon singlet → singlet excitation at 300 nm. [b] Absolute emission quantum yield measured upon singlet → triplet excitation at 360 nm.

Usually, several Tb^{III} *f-f* transitions may be noticed within the 320 – 380 nm range, which makes it difficult for the proper selection of an excitation wavelength coming only from the ligand absorption. To work around such issue, it is feasible to assume that since only ligand bands are observed in the excitation spectrum, Figure 3 in the main text, then Tb^{III} *f-f* bands are weak and they barely contribute to the excited state population. To ensure such assumption, we measured the emission spectra of $[Tb_2(bza)_6(H_2O)_2]$ complex (Figure S11) lacking direct triplet population at 360 nm, and upon such excitation wavelength, no Tb^{III} emission takes place, confirming that *f-f* processes may be disregard. Also, if the measured QY was influenced by Tb^{III} *f-f* absorption, one should expect similar QY results for all Tb^{III} complexes shown in Table S8 upon 360 nm excitation, which is not observed.

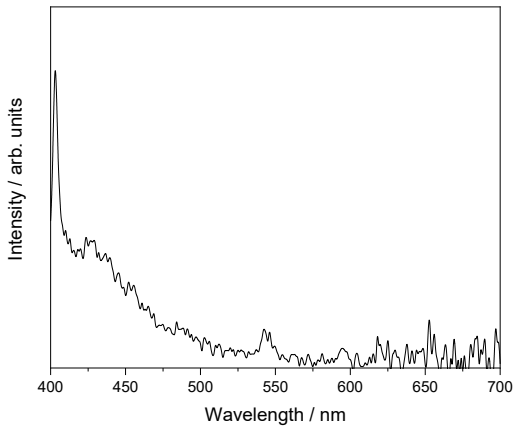

Figure S11. Emission spectrum of $[Tb_2(bza)_6(H_2O)_2]$ upon 360 nm excitation.

Supplementary note S8 – Photobleaching and thermal dependence of luminescence

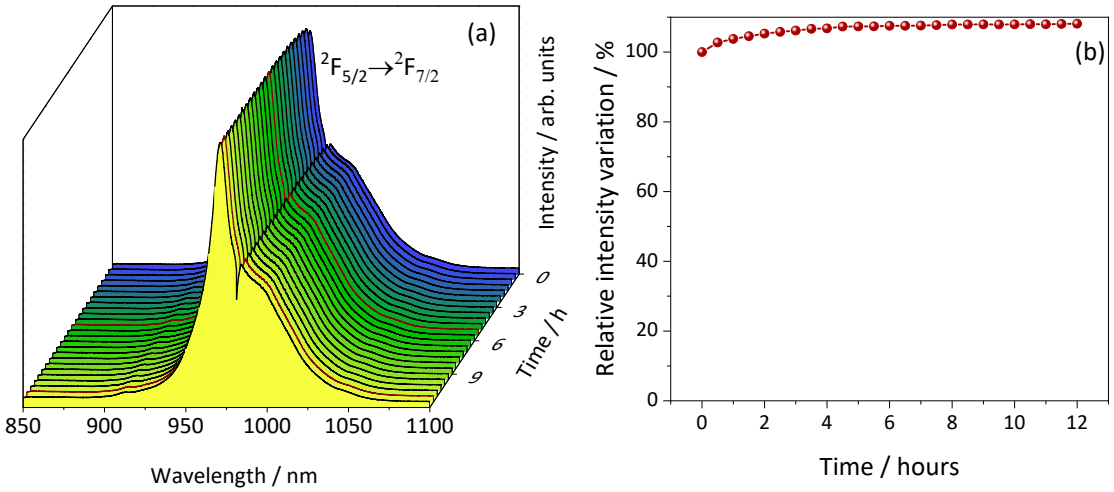

Figure S12. (a) Emission spectra of the $[Yb_2(3,5\text{-bbza})_6(H_2O)_2]$ complex monitored upon continuous 430 nm excitation (optical power of 2.8 mW, optical power density of 290 mW cm^{-2}) for 12 hours. (b) Relative integrated emission intensity of the $[Yb_2(3,5\text{-bbza})_6(H_2O)_2]$ complex.

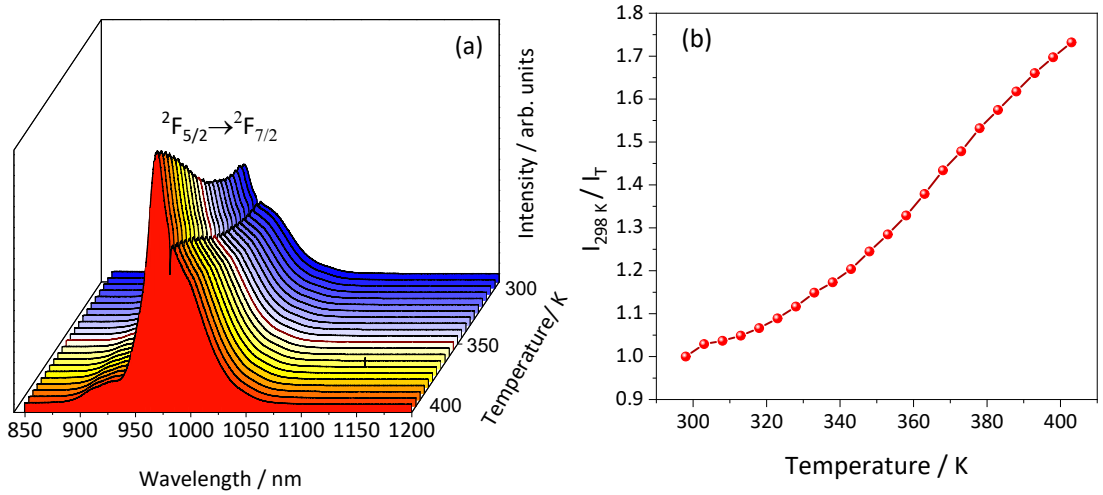

Figure S13. (a) Thermal dependence of luminescence within the 298 – 403 K range for the $[Yb_2(3,5\text{-bbza})_6(H_2O)_2]$ complex upon 430 nm excitation. Ratio of the integrated emission intensity at 298 K and at a temperature T.

Supplementary References

[1] K. Wittel, R. Manne, *Theoret. Chim. Acta (Berl.)* 1974, **33**, 347.
[2] S. Omagari, N. Takayuki, Y. Kitagawa, T. Seki, K. Fushimi, H. Ito, A. Meijerink, Y. Hasegawa, *J. Lumin.* 2018, **201**, 170.
[3] B. R. Judd, I. Lindgren, *Phys. Rev.* 1961, **122**, 1802.
[4] T. Koubaa, M. Dammak, M. Kammoun, W. M. Jadwisienczak, H. J. Lozykowski, A. Anders, *J. Appl. Phys.* 2009, **106**, 013106.
[5] J. H. S. K. Monteiro, A. Bettencourt-Dias, I. O. Mazali, F. A. Sigoli, *New J. Chem.* 2015, **39**, 1883.
[6] C. Würth, M. Grabolle, J. Pauli, M.Spieles, U. Resch-Genger, *Nat. Protoc.* 2013, **8**, 1535.
[7] J. D. L. Dutra, T. D. Bispo, R. O. Freire, *J. Comput. Chem.* 2014, **35**, 772.
[8] Stewart, J. P. MOPAC2012, Stewart Computational Chemistry, Version 15.217W.
[9] M. A. M. Filho, J. D. L. Dutra, G. B. Rocha, R. O. Freire, A. M. Simas, RSC Adv., 2013, **3**, 16747.
[10] F. Neese, *Rev. Comput. Mol. Sci.* 2012, **2**, 73.
[11] G. B. Deacon, R. J. Phillips*, Chem. Rev.* 1980, **33**, 227-250.
[12] R. T. Moura-Jr, A. N. Carneiro Neto, R. L. Longo, O. L. Malta, *J. Lumin.* **2016**, *170*, 420.
[13] A. Beeby, I. M. Clarkson, R. S. Dickins, S. Faulkner, D. Parker, L. Royle, A. S. de Sousa, J. A. Gareth Williams, M. Woods, *J. Chem. Soc., Perkin Trans.* 1999, **2**, 493.